Localized waveguide formation in germanosilicate fiber transmitting femtosecond IR pulses

Haohua Tu,[1],* Yee Lin Koh,[1] Daniel L. Marks,[1] and Stephen A. Boppart[1,2]

[1]*Biophotonics Imaging Laboratory, Beckman Institute for Advanced Science and Technology,*
University of Illinois at Urbana-Champaign, Urbana, Illinois 61801, USA
[2]*E-mail: boppart@uiuc.edu*
*Corresponding author: htu@uiuc.edu

Transmission of intense femtosecond 825 nm pulses progressively produces a waveguide at the entrance of a heavily Ge-doped silicate fiber. The waveguide behaves as a multimillimeter long-fiber bandpass filter that scatters away light with wavelengths shorter or longer than 850 nm. This phenomenon has been correlated with the ~800 nm photosensitivity producing type I-IR fiber Bragg gratings in side-written lightly Ge-doped silicate fibers and low-loss waveguides in pure silica bulk glass. A model incorporating color center formation is proposed to understand the underlying mechanism. © 2008 Optical Society of America

OCIS codes: 190.7110, 190.4370, 160.2750, 140.3390.

1. INTRODUCTION

Femtosecond (fs) ~800 nm IR irradiation from Ti:sapphire lasers may produce persistent refractive index modulation of pure or Ge-doped silica glass without causing material breakdown [1]. This photosensitivity has facilitated the microlithography of various photonic devices with properties similar to those made by conventional UV irradiation [2,3]. Although the multiphoton advantage of the IR approach is widely recognized, the underlying mechanism remains largely unknown [1,2]. A recent spectroscopic study [4] proposed the five-photon absorption of an oxygen deficiency center (ODC) to be responsible for writing low-loss three-dimensional waveguides [2]. However, another study [3] attributed the inscription of type I-IR fiber Bragg grating (FBG) to the five-photon assisted interband transition of glass. Although these interpretations attributed the photosensitivity to the formation of microscopic photoproducts termed as color centers, a competing class of interpretations attributed the photosensitivity to material macroscopic changes such as densification [5] and stress [6]. Neither class has quantitatively accounted for the observed refractive index modulation [1], just like their UV counterparts [7].

While the IR microlithography promotes the photosensitivity of refractive index modulation, the application of IR fiber lasers strives to reduce the photosensitivity of the rare-earth doped silica fibers [8]. Since absorptive species are photoinduced, this photosensitivity is termed as the photodarkening effect. The darkening rate may depend on the IR pump power to the fourth or fifth order, enabling the underlying mechanisms to be interpreted as certain multiphoton-assisted transitions and color center formations of the rare-earth dopants [9,10]. These dopants allow the photodarkening to occur at a peak pulse-intensity orders of magnitude lower than the TW/cm^2-scale intensities employed in the IR microlithography. A natural question arises if a similar effect exists in pure or Ge-doped silica fibers when this intensity attains TW/cm^2-scale, and if it does, whether it is related to the photosensitivity of the IR microlithography. In fact, supercontinuum has been generated in photonic crystal fibers (PCFs) [11], tapered fibers [12], and ultrahigh numerical aperture (UHNA) fibers [13] by TW/cm^2-scale fs IR pulses, and has found wide applications in metrology, spectroscopy, and optical imaging. However, few studies have been dedicated to the photosensitivity of these fibers (possibly because this will potentially limit the intended applications). We report here the observation of waveguide formation in a UHNA fiber and the correlation of this effect with the IR microlithography.

2. EXPERIMENT

We investigated two fiber types, a germanosilicate UHNA fiber (UHNA3, Nufern, East Granby, Connecticut) having a second mode cutoff wavelength of 900 ± 50 nm, and an endlessly single-mode PCF (LMA-8, Crystal Fibre A/S, Denmark) consisting of pure silica. Each has a silica cladding diameter of 125 μm and an acrylate coating diameter of 250 μm. UHNA3 and LMA-8 have NAs of 0.35 and 0.10 and mode field diameters of 2.0 and 6.0 μm (at 825 nm), respectively. UHNA3 has a step-index-type germanosilicate core, allowing Ge concentration to be estimated as 29 mol% [14]. The 120 fs 80 MHz pulses from a tunable Ti:sapphire laser (Mai Tai HP, Spectra-Physics, Mountain View, California) served as the pumping and probing source with ~10 nm bandwidth. The 1.2 mm diameter laser beam sequentially passed through a Faraday isolator, a neutral-density filter (NDF), an aspheric lens, and the entrance facet of a fiber having a length of 5−50 mm stripped of its acrylate jacket. The total fiber length was 2−5 m, with the first 100 mm mounted straight on a three-axis fiber positioner. A 0.65 NA, 3.6 mm clear aperture lens (C390TM, Thorlabs, Newton,

New Jersey) was used for UHNA3, while a 0.40 NA, 5.0 mm clear aperture lens (C110TME, Thorlabs, Newton, New Jersey) was used for LMA-8. The fact that the laser beam diameter is smaller than the clear aperture of the lens compensates the NA mismatch between the lenses and fibers, resulting in 60–70% coupling efficiency (CE) of the incident energy for both fibers. CE was measured to be the ratio of the maximized power exiting from the fiber (P_{out}) to the power before entering the fiber (P_{in}), assuming negligible loss in the short fiber length. In this measurement, P_{in} was attenuated to 50 mW by the NDF to avoid multiphoton-induced CE change (as described below). The corresponding coupling loss was assessed by measuring the scattered light along a fixed direction from the mounted fiber section about 40–90 mm from the entrance facet. The fiber-optic probe of a spectrometer (USB4000, Ocean Optics) was mounted on a three-dimensional positioner to vertically approach the fiber within ~0.5 mm and record the spectrum of the scattered light. The CE data as a function of probing wavelength (λ_{probe}) is termed as the CE spectrum (CES). The CES of a freshly cleaved UHNA3 or LMA-8 fiber is highly reproducible, while CE is nearly independent of λ_{probe} across 725–925 nm. This provides an excellent reference to study CES-related photosensitivity due to the supercontinuum generation process, in which the pumping wavelength (λ_{pump}) was varied across 780–910 nm while the pumping power P_{in} was typically above 200 mW. This process was initiated by first maximizing CE at low P_{in} and then increasing P_{in} to the desired power. CE is smaller at higher P_{in}, but the difference is typically no more than 10%.

3. RESULTS

Figures 1(a) and 1(c) are characteristic of the observed CES of a fresh UHNA3 fiber before and after typical uninterrupted supercontinuum-generating processes at λ_{pump}=825 nm. During the processes, the initial P_{out} drops by ~18% (which cannot be compensated by optical realignment), while the CES evolves into a filter-like profile peaked at 850 nm. This effect reflects a change of linear optical property, because the same measurement using 50 mW cw light with ~1 nm bandwidth (produced by cw operation of the same laser) generates the same CES. Although the CES is measured by pulsed probing light with 25 nm increments across 725–925 nm, the more accurate measurement based on the cw light with 2 nm increments has not resolved any fine CES structures across this spectral region. The effect is persistent over a fiber storage time of >5 days. The modification is restricted to within 10 mm from the fiber entrance facet, as the removal of this length by fiber cleaving provides a new facet with a CES approximating that of a freshly cleaved fiber. Thus the localized modification is associated with high-peak-pulse intensity that is reduced during propagation by normal dispersion along the fiber, and the modified region of the fiber core is termed the nonlinear section. On the other hand, the scope of the modification extends beyond 1 mm from the fiber entrance facet, as the removal of this length by fiber polishing results in little CES increase.
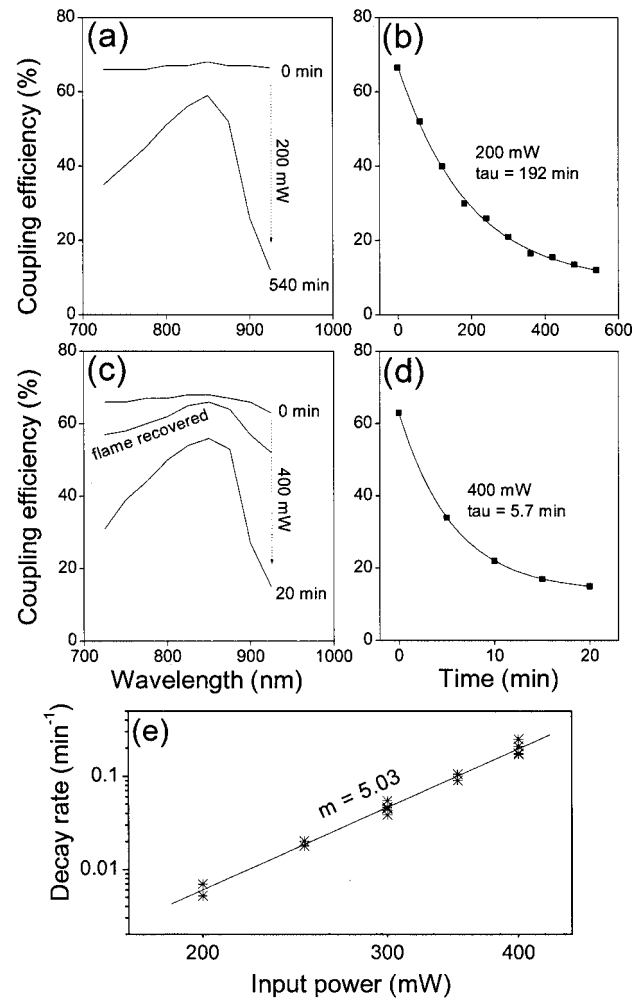
Fig. 1. (a) CES of a UHNA3 fiber when freshly prepared and light treated (825 nm, 200 mW, 540 min); (b) CE kinetics of (a) at 925 nm (dot) and corresponding first order exponential decay fit (curve); (c) CES of another UHNA3 fiber when freshly prepared, light treated (825 nm, 400 mW, 20 min), and flame recovered; (d) CE kinetics of (c) at 925 nm (dot) and corresponding first-order exponential decay fit (curve); (e) double-logarithmic plot of decay rate τ^{-1} versus pump power P_{in} at λ_{probe}=925 nm.

A plausible explanation for the CES modification is the relaxation of the internal stress of the fresh fiber with high-intensity exposure, as the highly Ge-doped UHNA3 fiber may be under large internal stress owing to material mismatch between the core and cladding. However, such relief of the stress should increase rather than decrease CE. It should be noted that the PCF has a nearly identical CES profile (i.e., flat across 725–925 nm) as the UHNA fiber but has no stress owing to the material mismatch. This fact suggests that a fresh UHNA3 fiber has minimum stress. After the nonlinear section of the above light-treated fiber is heated with a candle flame (T=1620 K) for ~1 min, the CES of the fiber is recovered to that of a fresh fiber [Fig. 1(c)], and the recovered fiber behaves similarly to a freshly cleaved fiber. A complete recovery may be achieved by optimizing the heating procedure. Thus, the stress (if any) may be induced (rather than relieved) by the light treatment and subsequently relieved by the flame treatment.

Similar CES change can be attained at λ_{pump} across 780–840 nm with a wide range of P_{in} and exposure time. This motivates us to evaluate the dependence of CE decay kinetics on P_{in}. The CE decay kinetics of a fresh UHNA3 fiber are plotted in Figs. 1(b) ($P_{in}=200$ mW) and 1(d) ($P_{in}=400$ mW) at $\lambda_{pump}=825$ nm and $\lambda_{probe}=925$ nm. The corresponding measurements are conducted at periodical interruptions when the laser wavelength is switched from λ_{pump} to λ_{probe}. Once the CE is measured, the wavelength is switched back to λ_{pump}, the CE is maximized, and P_{in} is increased to resume the optical processing. Comparative results of interrupted and uninterrupted experiments exclude any effects of these measurement interruptions on the kinetics. For a P_{in} of 200–400 mW, the CE decay kinetics can be well fitted to an exponential decay of $Ae^{-t/\tau}+C$ with a P_{in}-independent amplitude A of $51\pm4\%$ and constant C of $13\pm3\%$, along with a P_{in}-dependent decay time constant τ [Figs. 1(b), 1(d), and 1(e)]. In the same experiments, the kinetics at $\lambda_{probe}=725$ nm can also be well fitted to an exponential decay with a τ approximating that at $\lambda_{probe}=925$ nm (within 10%), although with different A and C constants. This suggests that the modified CES is the spectroscopic signature of a single photoproduct. Since the induced CE loss is low at $\lambda_{pump}=825$ nm (15–22%), the nonlinear section of the fiber is effectively exposed to a constant intensity proportional to P_{in}. The double-logarithmic plot of decay rate τ^{-1} versus P_{in} reveals a linear relation of a slope of 5.03 [Fig. 1(e)], indicating the presence of a five-photon assisted process [9,10].

The CE loss of the fiber cannot be attributed to the absorption of the photoproduct because the absorption volume is too small to avoid destructive thermal effects. In the measurement interruptions of the above kinetic experiments, the scattering intensity at $\lambda_{probe}=925$ nm (i.e., integrated spectral area across 900–960 nm) recorded by the spectrometer is found to increase with decreasing CE, as demonstrated in Fig. 2(a). Thus the CE loss is originating from scattering. Analogous to the photodarkening effect, the phenomenon can be termed as the photoscattering effect. Thus the modified nonlinear section of the fiber responsible for this effect behaves as a waveguide. In the experiment associated with Fig. 2(a), the scattering intensity at each pumping time, if scaled by a common constant, may complement its corresponding CE to produce a sum of $96.0\pm1.6\%$ [Fig. 2(b)], $100.0\pm2.1\%$, or $92.0\pm2.0\%$. It should be noted that significant scattering intensity can be detected only at fiber locations where the acrylate coating is not stripped off. This indicates that the scattered light comes from the diffusive cladding-coating interface and should be proportional to the intensity of the light propagated along the cladding at the probed location. Thus the validity of the 96.0% scaling with the minimum standard deviation of 1.6% can be justified if the Fresnel reflection at the fiber entrance facet accounts for a loss of 4%, and the decreasing CE (i.e., increasing scattering intensity) is due to the redistribution of the light energy from the core (fundamental) mode to the cladding modes. This redistribution is induced by the waveguide that scatters the propagating core mode with scattering angles between 13° to 48° (the light that can be totally reflected in the cladding but not the core). The propagating
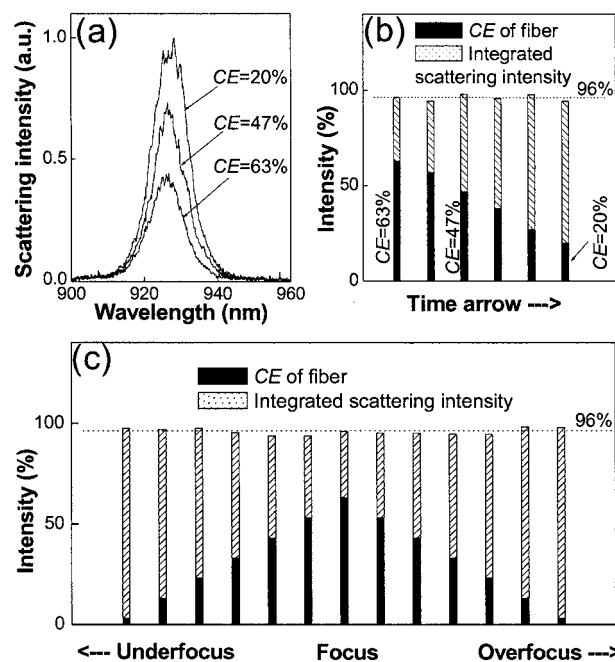
Fig. 2.   (a) Spectra of the scattered light collected by a fiber-optic spectrometer at several instances of CE ($\lambda_{probe}=925$ nm); (b) complimentary correspondence between the scaled scattering intensity and corresponding CE in (a) with increasing pumping time; (c) complimentary correspondence between the scaled scattered intensity and corresponding CE in (b) at the under-focus or over-focus conditions of the aspheric lens before pumping.

cladding modes lose energy along the fiber due to the dissipative scattering and do not exit from the end of the fiber. This explanation implies that the blank (initial) coupling loss of 33% in Fig. 2(b) can only be attributed to the aspheric lens that distributes the energy of the focused Gaussian beam between the core and the cladding. To confirm this, the scattering intensity and the CE are monitored when the freshly cleaved fiber is moved slightly ($<50\,\mu$m) toward (over-focus) or away from (under-focus) the aspheric lens. Again, the scattering intensity can be scaled to similarly compliment the corresponding CE (Fig. 2(c)). Because the Gaussian beam waist ($\sim1\,\mu$m) is smaller than the mode field diameter of the fiber, either defocus condition diverges the beam coupled into the fiber core to increase the coupling loss [Fig. 2(c)]. The similarity between Figs. 2(b) and 2(c) illustrates that the photoinduced waveguide effectively diverges (scatters) the beam coupled into the fiber core, just like the two defocus conditions. Similar results have been obtained at $\lambda_{probe}=725$ nm and from other kinetic experiments in which the scattered light is measured at somewhat different fiber locations along somewhat different scattering directions. Thus, the magnitude of the recorded scattered light intensity along one scattering direction reflects that of the scattered light intensity integrated over all scattering directions. The occurrence of the minimum scattering at $\lambda_{probe}=850$ nm [Fig. 1(a)] may be related to the specific structure of the waveguide.

The effort to identify the waveguide by scanning electron microscopy (SEM) has not been successful as the SEM image from the light treated fiber [Fig. 1(c)] differs little from that of a freshly cleaved UHNA3 fiber. How-

ever, photoinduced damages have been found at the entrance facet near the core of a UHNA3 fiber after prolonged 825 nm pumping (Fig. 3). Because a 60 times larger irradiation dosage is used to induce such damages, we make no judgment whether the corresponding photosensitivity is related to that responsible for the CES modification [Fig. 1(c)].

4. DISCUSSIONS

The five-photon process attenuating the fiber transmission resembles the five-photon process writing low-loss waveguides in bulk silica glass [2,4] and the five-photon process producing type I-IR FBGs in telecommunication fibers (known to have a 3 mol% Ge-doped silica core [15]) [3]. Both features can be erased by annealing, just like the waveguide observed in this study. Peak pulse intensity thresholds to induce the waveguides and the FBGs are found to be 7.96 and $18 \, \text{TW/cm}^2$, respectively. These thresholds are defined by experimental sensitivity rather arbitrarily because of the high-order power dependence. In the waveguide case, a second threshold is found at $9.15 \, \text{TW/cm}^2$ [4], which results in high-loss waveguides [2]. In the FBG case, a similar second intensity threshold is found at $46 \, \text{TW/cm}^2$, which produces thermally stable type II-IR FBG [3]. To examine the existence of such a dramatic threshold in a freshly cleaved UHNA3 fiber, we first optimize CE at a fixed λ_{pump} (750–910 nm), and monitor P_{out} while gradually increasing P_{in}. Indeed, P_{out} suddenly drops from $>300 \, \text{mW}$ to $\sim 50 \, \text{mW}$ when P_{in} passes a threshold value. The threshold powers at λ_{pump} of 750 nm, 800 nm, 850 nm, and 950 nm are 750 mW, 855 mW, 960 mW, and 1090 mW, respectively, with a typical standard deviation of 50 mW. It should be noted that the spot size of the focusing aspheric lens depends on λ_{pump}. Assuming the 120 fs laser pulses are elongated to 300 fs immediately before entering the fiber, we calculate the spot-size adjusted threshold to be $\sim 2 \, \text{TW/cm}^2$, independent of λ_{pump}. This independence is consistent with the avalanche breakdown model [16]. The damage is

Fig. 3. (left) SEM image of the entrance facet of a freshly cleaved fiber near the germanosilicate core, the scale bar represents 2 μm; (right) SEM image of the entrance facet of an irradiated fiber (825 nm, $\sim 400 \, \text{mW}$, 20 h in five days) near the germanosilicate core.

found to be restricted within 1 mm from the fiber entrance facet and can not be reversed by a $\sim 1 \, \text{min}$ candle flame treatment.

The striking coincidences discussed above strongly suggest the occurrence of the same pair of distinct processes at a pair of intensity thresholds. The reversible process associated with the lower threshold induces low-loss but thermally unstable photonic features, while the irreversible one associated with the higher threshold induces thermally stable but high-loss features. The irreversible process is due to the avalanche breakdown rather than the multiphoton-assisted disruption of a certain strained bond [4], which should somewhat depend on λ_{pump}. The fact that no CES modification is induced at λ_{pump} = 860 nm with comparable pumping intensities makes it unfavorable to attribute the reversible process to the five-photon assisted interband transition [3]. Five 860 nm photons have a total energy of 7.2 eV, which is more than adequate to bridge the bandgap of the heavily Ge-doped silica glass of UHNA3 (between 5.6 to 7.1 eV [15]). The reversible process is alternatively attributed to the five-photon absorption of the ODC of silica glass (SiODC, i.e., $\equiv$Si-Si$\equiv$) in the waveguide case as suggested before [4], or a combination of SiODC and GeODC ($\equiv$Ge-Si$\equiv$ or $\equiv$Ge-Ge$\equiv$) in the fiber cases. The singlet–singlet ($S_0 - S_1$) transition of SiODC is well known to be responsible for a 7.6 eV absorption band [17], and the energy of the $S_0 - S_1$ transition is nearly identical for SiODC and GeODC [18]. Thus, the five-photon absorption of 800 nm (1.55 eV) or 825 nm (1.50 eV) radiation excites the transition of these ODCs to stimulate the reversible process.

The above damage threshold analysis implies that the thermally reversible CES modification is induced at threshold intensity below $0.5 \, \text{TW/cm}^2$ (i.e., 200 mW) for 825 nm pumping. In the comparative experiments using the PCF, the maximum power allowed by the laser at 825 nm (2.0 W) is used to pump the fiber, resulting in an intensity of $0.5 \, \text{TW/cm}^2$. However, 600 min of such pumping does not change the CES of the fiber. This indicates that the light-induced CES modification of the UHNA3 fiber is primarily due to the five-photon assisted excitation of GeODC. During the excitation, GeODC produces an E' color center known as the dominant species of the refractive index modulation [17] and an energized electron [4] whose fast relaxation may transfer its energy to the glass matrix [7]. The refractive index modulation of the color center should be relatively homogeneous in the nonlinear section of the fiber. It is unlikely that this modulation alone produces the waveguide with CES of dramatic CE wavelength dependence. It is more likely that the energy transferred to the glass matrix results in a macroscopic structural change in the nonlinear section of the fiber, leading to a heterogeneous refractive index modulation through mechanisms such as densification [5] or stress [6]. Alternatively, the heterogeneous refractive index modulation in the nonlinear section of the fiber may be caused by the formation of a structure analogous to long period grating (LPG). This structure is possibly generated by interference between the core and cladding modes in the nonlinear section of the fiber and can attenuate light transmission at particular probing wavelength by coupling the core mode into the cladding modes. The struc-

ture is not a strict LPG, because it exhibits a broad transmission band rather than a narrow attenuation band.
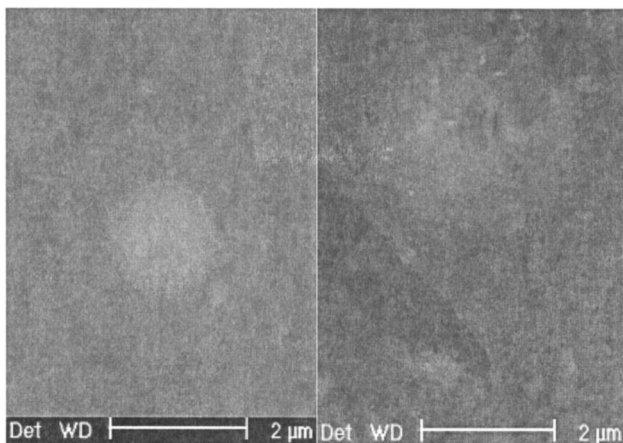
5. CONCLUSIONS

A multimillimeter-long waveguide forms in a normally dispersive germanosilicate fiber during supercontinuum generation. The waveguide behaves as a nonabsorptive bandpass fiber filter that selectively passes ∼850 nm light. The photosensitivity that produces this waveguide has been linked to that which produces the low-loss waveguides and type I-IR FBGs in IR microlithography. Thus this photosensitivity can be enhanced by increasing the concentration of ODCs in raw materials. The properties of the waveguide may be engineered by fiber preparation to make new photonic devices. On the other hand, the photosensitivity inevitably affects the stable operation of fiber-optic supercontinuum sources and may be suppressed by removing the ODCs using UV irradiation or oxygen oxidization.

ACKNOWLEDGEMENTS

REFERENCES

1. A. M. Streltsov and N. F. Borrelli, "Study of femtosecond-laser-written waveguides in glasses," J. Opt. Soc. Am. B **19**, 2496–2504 (2002).
2. A. Zoubir, M. Richardson, L. Canioni, A. Brocas, and L. Sarger, "Optical properties of infrared femtosecond laser-modified fused silica and application to waveguide fabrication," J. Opt. Soc. Am. B **22**, 2138–2143 (2005).
3. C. Smelser, S. Mihailov, and D. Grobnic, "Formation of type I-IR and type II-IR gratings with an ultrafast IR laser and a phase mask," Opt. Express **13**, 5377–5386 (2005).
4. A. Zoubir, C. Rivero, R. Grodsky, K. Richardson, M. Richardson, T. Cardinal, and M. Couzi, "Laser-induced defects in fused silica by femtosecond IR irradiation," Phys. Rev. B **73**, 224117 (2006).
5. J. W. Chan, T. Huser, S. Risbud, and D. M. Krol, "Structural changes in fused silica after exposure to focused femtosecond laser pulses," Opt. Lett. **26**, 1726–1728 (2001).
6. V. R. Bhardwaj, P. B. Corkum, D. M. Rayner, C. Hnatovsky, E. Simova, and R. S. Taylor, "Stress in femtosecond-laser-written waveguides in fused silica," Opt. Lett. **29**, 1312–1314 (2004).
7. M. Kristensen, "Ultraviolet-light-induced processes in germanium-doped silica," Phys. Rev. B **64**, 144201 (2001).
8. J. J. Koponen, M. J. Söderlund, H. J. Hoffman, and S. K. T. Tammela, "Measuring photodarkening from single-mode ytterbium doped silica fibers," Opt. Express **14**, 11539–11544 (2006).
9. M. M. Broer, D. M. Krol, and D. J. DiGiovanni, "Highly nonlinear near-resonant photodarkening in a thulium-doped aluminosilicate glass fiber," Opt. Lett. **18**, 799–801 (1993).
10. P. Laperle, A. Chandonnet, and R. Vallee, "Photoinduced absorption in thulium-doped ZBLAN fibers," Opt. Lett. **20**, 2484–2486 (1995).
11. J. K. Ranka, R. S. Windeler, and A. J. Stentz, "Visible continuum generation in air-silica microstructure optical fibers with anomalous dispersion at 800 nm," Opt. Lett. **25**, 25–27 (2000).
12. T. A. Birks, W. J. Wadsworth, and P. St. J. Russell, "Supercontinuum generation in tapered fibers," Opt. Lett. **25**, 1415–1417 (2000).
13. D. L. Marks, A. L. Oldenburg, J. J. Reynolds, and S. A. Boppart, "Study of an ultrahigh-numerical-aperture fiber continuum generation source for optical coherence tomography," Opt. Lett. **27**, 2010–2012 (2002).
14. A. S. Huang, Y. Arie, C. C. Neil, and J. M. Hammer, "Study of refractive index of GeO2:SiO2 mixtures using deposited-thin-film optical waveguides," Appl. Opt. **24**, 4404–4407 (1985).
15. D. N. Nikogosyan, "Multi-photon high-excitation-energy approach to fibre grating inscription," Meas. Sci. Technol. **18**, R1–R29 (2007).
16. R. W. Boyd, *Nonlinear Optics* (Academic, 2003), p. 517.
17. L. Skuja, "Optically active oxygen-deficiency-related centers in amorphous silicon dioxide," J. Non-Cryst. Solids **239**, 16–48 (1998).
18. B. B. Stefanov and K. Raghavachari, "Photoabsorption of the neutral oxygen vacancy in silicate and germanosilicate glasses: first-principles calculations," Phys. Rev. B **56**, 5035–5038 (1997).